Science and Technology Indonesia
e-ISSN:2580-4391 *p*-ISSN:2580-4405
Vol. 5, No. 3, July 2020

Research Paper

Transesterification Reaction from Rice Bran Oil to Biodiesel over Heterogeneous Base Calcium Oxide Nanoparticles Catalyst

Nur Fatin Sulaiman[1], Abdul Rahim Yacob[1], Siew Ling Lee[1,2]*

[1] *Department of Chemistry, Faculty of Science, Universiti Teknologi Malaysia, 81310 Johor Bahru, MALAYSIA*
[2] *Centre for Sustainable Nanomaterials, Ibnu Sina Institute for Scientific and Industrial Research, Universiti Teknologi Malaysia, 81310 Johor Bahru, MALAYSIA*
***Corresponding author**: lsling@utm.my

Abstract
This study focuses on the development of an alkaline earth metal oxide, calcium oxide (CaO) as heterogeneous base catalyst for biodiesel production. The intention for this study is to explore potential for the transformation of commercial calcium carbonate, CM-$CaCO_3$ into CaO nanoparticles and further used as a heterogeneous base catalyst in single step transesterification reaction from rice bran oil to biodiesel. The prepared CaO was calcined under 10^{-3} mbar vacuum, at temperatures ranging from 100°C to 700°C. TGA-DTA results revealed that the CM-$CaCO_3$ must be calcined above 600°C in order to form CaO. This is in accordance with FTIR results which specified the complete formation of CaO at 700°C. XRD revealed that the rhombohedral $CaCO_3$ and hexagonal $Ca(OH)_2$ had completely been disappeared, leaving only crystalline cubic CaO at 700°C. Interestingly, the larger BET surface area (11.5 m^2g^{-1}) and highest basicity (1.959 mmol/g) were observed for CaO calcined at 700°C (CaO-700). The CaO-700 nanoparticles were designated as a catalyst for the transesterification reaction of rice bran oil to give biodiesel. NMR and GC-FID results further confirmed the successful formation of biodiesel using CaO-700 as catalyst.

Keywords
Heterogeneous Catalyst; Nanoparticles; Biodiesel; Transesterification

Received: 14 June 2020, Accepted: 13 July 2020
https://doi.org/10.26554/sti.2020.5.3.62-69

1. INTRODUCTION

The physicochemical characteristics of a heterogeneous catalyst depend on their preparation techniques and the primary treatment process. There are many of research techniques are available to produce solid base catalyst such as hydration dehydration method (Aziz et al. (2012); Yacob and Sulaiman (2012)), sol gel (Corrêa et al. (2020)) and chemical vapor deposition (CVD) methods (Knözinger et al., 2000). In general, physical and chemical properties such as surface area, particle size, morphology and basicity would affect each of catalytic activity. The significance of heterogeneous base catalysts also became recognized for their environmentally sustainable qualities. Much significant progress in catalytic materials and solid base-catalyzed reactions has been made over the past two decades (Hattori, 2001)

It was reported by Hattori (2001), a strong basic strength of carbonate-free metal oxide surfaces could be developed after a high-temperature treatment. Surface defect that was detected by nitrogen adsorption analysis demonstrated important heterogeneous catalytic sites that could enhance the reactivity of each reaction (Boro et al., 2012). As a result, the larger surface area implied good reactivity. Alkaline earth metal oxides including calcium oxide, CaO has basic characteristics as its oxides provide basic alkaline solutions when mixed with water. By transforming the basic oxide to hydroxides, the proton was transmitted from water to basic oxide. Alternatively, the solid basic oxides donated their electron pair to the reactants. It was documented that the alkaline earth metal oxide acted as a Brönsted base, while the water functioned as a Brönsted acid. In the biodiesel production, transesterification reaction is the most widely studied utilizing alkaline earth metal oxide as solid base catalyst (Mazaheri et al. (2018); Dawood et al. (2018); Shan et al. (2016)).

Biodiesel as one of the renewable energies can be produced from vegetable oils or animal fats. It consists of blend of long-chain alkyl esters such as methyl esters, which are used without modification to the diesel engine as an alternative for petroleum oil. By using above resources, this biodiesel consisting of fatty acid alkyl ester is generally produced by transesterification reaction. There are number of techniques to perform this reaction including supercritical process, common batch process, ultrasonic technique and microwave method (Rathnam et al. (2020); Hakim et al. (2019); Sharma et al. (2019)).

This present study focused on the preparation of CaO nanoparticles from commercial calcium carbonate, CM-$CaCO_3$ under

vacuum atmosphere of 10^{-3} mbar at 100 to 800°C by thermal decomposition process. The basicity of the CaO nanoparticles was examined using back-titration method in order to investigate the relationship between basicity and calcination temperature. The prepared CaO nanoparticles were then used for the transesterification of rice bran oil to biodiesel as a heterogeneous base catalyst. Rice bran oil has been selected as it is unconventional, low-cost and low-grade vegetable oil that does not have much competition for food requirement.

2. EXPERIMENTAL SECTION

2.1 Materials

In this research, the chemical reagents were used such as commercial calcium carbonate, $CaCO_3$, hydrochloric acid, HCl, sodium hydroxide, NaOH, methanol, CH_3OH and n-hexane, C_6H_{14} with molecular weight 100.09 g/mol, 36.46 g/mol, 40.00 g/mol, 32.04 g/mol and 86.07 g/mol, respectively. All chemical reagents were purchased from QRëC. The rice bran oil, acquired from the local store was used for the transesterification reaction.

2.2 Catalysts Preparation

Calcium oxide, CaO nanoparticles were prepared using thermal decomposition method under vacuum atmosphere at various calcination temperatures ranging 100 to 800 °C. The samples were labeled as CaO-100 to CaO-800 according to their calcination temperature. Approximately 0.4 g of the commercial $CaCO_3$ powder was inserted in a quartz tube attached to vacuum line system. CM-$CaCO_3$ precursor was calcined at 100 to 800 °C in 10-3 mbar vacuum for 2 hours to produce about 0.2 g of CaO sample. The basicity of CaO nanoparticles was determined via back-titration method. For this purpose, CaO (100 mg) was dissolved in 10 mL of distilled water. After left for 24 hours, the slurry was obtained and then centrifuged. Neutralization of the resulting solution was performed using 0.05 M HCl (10 mL). Finally, titration with phenolphthalein as an indicator was carried out using NaOH (0.02 M) for the remaining acid (Yacob and Sulaiman, 2012).

2.3 Catalysts Characterizations

The prepared CaO samples were characterized by using thermogravimetric analysis–differential thermal analysis (TGA-DTA), Fourier transform infrared (FTIR), X-ray diffraction (XRD), field emission scanning electron microscopy (FESEM), energy dispersive X-ray (EDX) and nitrogen adsorption analysis (NA). The decomposition of $CaCO_3$ was studied from TGA-DTA analysis using Mettler-Toledo Q100 instrument. About 15 mg sample was placed in a ceramic crucible and heated at temperature of 60 to 1000 °C at 15 °C/min with the flow rate 50 mL/min of nitrogen gas. TGA analysis was performed to confirm the optimum activation temperature in the preparation of CaO. Next, Fourier Transform Infrared Spectroscopy (FTIR) technique (wavenumber from 4000 to 400 cm^{-1}) from Shimadzu 8300 was used to identify the functional groups (CM-$CaCO_3$ and CaO samples). XRD analysis was carried out to examine the crystallinity degree, crystal structure and crystallite size of $CaCO_3$ and the prepared CaO samples. The XRD diffractograms were obtained on a Siemens D5000 powder instrument using Cu-Kα radiation (λ = 0.15148 nm; kV = 40; mA = 40) with the 2θ range from 10° to 90°.

Monosorb Surface Area Analyzer model was used to evaluate the surface area of the prepared CaO samples. Prior to the analysis, powder sample (0.1 g) was degassed at 120 °C for 2 hours by vacuum pump to cool down the sample at room temperature. This treatment was performed to remove adsorbed gases and dead space. Besides, FESEM was used to examine the surface morphology, particles size and shape on the surface of CaO samples via Zeiss Supra 35 VP scanning electron microscope. The CaO samples were placed on the carbon dual-sided tape aluminum stub in a small vacuum chamber. All the CaO samples were coated with gold before the FESEM analysis. The elemental composition of the samples was confirmed through EDX analysis.

2.4 Catalytic Transesterification Reaction

In the catalytic transesterification reaction, the prepared CaO (0.1 g) together with 15.0 g of methanol and 10.0 g of rice bran oil were added into a two-neck round bottle flask. The mixture was refluxed at 65 ± 5 °C for 30 min, followed by cooling process at ambient temperature. The mixture was then centrifuged at 5000 rpm for 10 min to separate the solid catalyst from the solution. Three layers were obtained which consisted of an excess of methanol (top layer), a biodiesel (middle layer) and CaO with glycerol (bottom layer). The first and second layers were collected and placed into a separating funnel in order to separate the biodiesel and methanol. The biodiesel was collected for further characterization.

2.5 Product Analysis

The quantitative production of biodiesel was identified by nuclear magnetic resonance (NMR). Methyl esters derived from the transesterification reaction were analyzed by ^{1}H NMR in $CDCl_3$ using TMS as internal standard. The ratio between the peak of 3.6 ppm from methoxyl groups of methyl esters and 2.3 ppm from α-carbon CH_2 groups of all fatty acid derivatives was used to calculate the percentage yield of methyl ester. Meanwhile, the chemical composition of volatile and its abundance of biodiesel produced was determined using gas chromatography (GC) recorded from Hewlett Packard Gas Chromatography model 6890. Helium gas was used as the mobile phase and column DB-Wax with specification 0.25 μm thicknesses, 30 m length and 0.20 mm internal diameter as the stationary phase with Flame Ionization Detector (FID). The dilution of biodiesel to n-hexane was 1:5 mL. The injector temperature rate was set at 40°C/5 min and the detector temperature was fixed at 300 °C for 15 minutes. The temperature was programmed at 5°C/min and the flow rate was 10 mL/min. For this product analysis, approximately 1 μL of this mixture was injected into the GC.

3. RESULTS AND DISCUSSION

3.1 Catalysts Characterizations

3.1.1 Thermogravimetric Analysis–Differential Thermal Analysis (TGA-DTA)

In the preparation of CaO samples, thermogram TGA-DTA for the optimum activation temperature was identified in the decomposition of $CaCO_3$. Figure 1 illustrates the percentage weight loss for the decomposition of $CaCO_3$ at different temperature regions. Based on Figure 1, there are four major weight loss that occurred from the decomposition of $CaCO_3$ to CaO at 60 to 700 °C. The first region occurred at temperature range of 60 to 100 °C was 1.6%. This occurrence was related to the removal of physically adsorbed water at $CaCO_3$ surface. The second region showed that the percentage weight loss occurred at 100 to 250 °C was 1.3% due to the loss of hydroxyl groups on the surface that attached to Ca^{2+}. Besides, the third region indicated the weight loss that occur at 250 to 600 °C was 1.4% due to the loss of carbonate group from $CaCO_3$. The major weight loss occurred at 600 to 700 °C about 3.4% was related to the decomposition of calcium carbonate, $CaCO_3$ to calcium oxide, CaO as in good agreement with Kristl et al. (2019). This weight loss implied the beginning formation of surface modified CaO from removal of carbon dioxide, CO_2 as the by-product. As shown in Figure 1, it could be inferred that decomposition of $CaCO_3$ to CaO occurred at temperature higher than 600 °C. Therefore, as the sample weight remained constant after 700 °C, this temperature was considered suitable for complete decomposition of $CaCO_3$ into CaO.

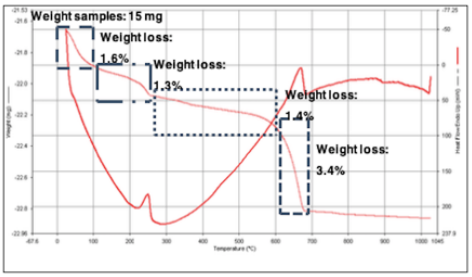

Figure 1. TGA-DTA profile of $CaCO_3$ sample

3.1.2 Fourier Transform Infrared (FTIR) Analysis

Figure 4 illustrates the FTIR spectra for all prepared CaO samples calcined at temperatures of 100 to 800 °C. The peak at 3640 cm^{-1} demonstrates that O-H bond stretching vibration at surface water attached to Ca^{2+}. As the temperature was increased from 100 to 800 °C, the band at 3640 cm^{-1} becomes smaller and disappeared. This indicated that the prepared CaO-700 did not contain water. This is in accordance with TGA-DTA data where the percentage weight loss occurred at temperature of 100 to 250 °C was most probably related with the loss of hydroxyl group at surface that attached to Ca^{2}+. The minor bands at 2920 cm^{-1} and 2870 cm^{-1} were corresponded to the C=O bond stretching vibration from carbonate ion. The thin and intense band at 1796 cm^{-1} was also associated to the carbonate C=O bond. As increasing the temperature from 100 to 800 °C, the peak became smaller and disappeared due to the loss of C=O bond from the formation of CaO. Besides, the very strong bands at 1400 cm^{-1}, 870 cm^{-1} and 848 cm^{-1} were related to the three different elongation modes of C-O bond bending vibration. The peak at 2513 cm^{-1} shows the harmonic vibration of these elongation modes for C-O bond bending vibration.

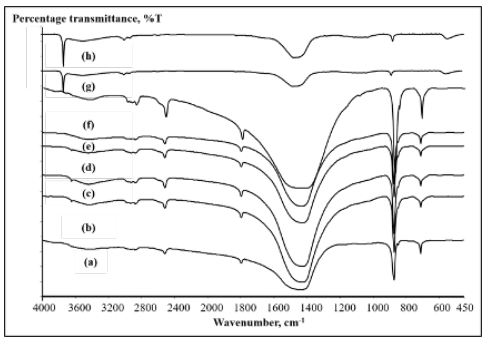

Figure 2. FTIR spectra of prepared CaO samples at various calcination temperatures of (a) CaO-100 at 100 °C, b) CaO-200 at 200 °C, (c) CaO-300 at 300 °C, (d) CaO-400 at 400 °C, (e) CaO-500 at 500 °C, (f) CaO-600 at 600 °C, (g) CaO-700 at 700 °C, and (h) CaO-800 at 800 °C

3.1.3 X-ray Diffraction (XRD) Analysis

Figure 3 shows the XRD diffractograms for all prepared CaO samples at different calcination temperatures from 100 to 700°C, while Table 1 represents XRD peaks assignment for CaO-600 and CaO-700. In this study, the temperature for decomposition of $CaCO_3$ to CaO was determined by referring to the TGA-DTA and FTIR data which shows the optimum temperature of forming CaO started at 600°C and above. Based on Figure 2, as the temperature increased, the hexagonal of $Ca(OH)_2$ peaks became smaller and the cubic CaO crystal started to appear. Finally, at 700°C, all the rhombohedral $CaCO_3$ and hexagonal $Ca(OH)_2$ totally disappeared and only cubic CaO was detected. This was probably due to the sintering effect which changes the sample characteristic and hydroxides group have been eliminated from the sample, thus completely converted to CaO (Li et al., 2020). Furthermore, the crystallite size for the prepared CaO nanoparticles was calculated using Sherrer's equation. The prepared surface modified CaO was truly at nano size as in accordance with (Duan et al., 2007). From the calculation, it was found that CaO-700 was completely in cubic crystal structure with crystallite size of 38 nm.

3.1.4 Nitrogen Adsorption Analysis (NA)

The specific BET surface area, SBET of CaO samples at different calcination temperatures are listed in Table 2. The SBET shows an increasing pattern of CaO samples as the temperature increased from 100 to 700 °C. The highest SBET obtained was CaO-700 with 11.5 m^2g^{-1}. The increased surface area could be

Table 1. XRD peaks assignment for CaO-600 and CaO-700

Sample	Angle, 2θ	d (Å)	d (Å) reference	Miller index, hkl hkl	Peaks Assignment
CaO-600	29.46	3.03	3.02	104	Rhombohedral
	32.23	2.77	2.78	111	Cubic
	37.36	2.41	2.41	200	Cubic
	53.88	1.7	1.7	220	Cubic
	64.21	1.45	1.45	311	Cubic
	67.47	1.39	1.39	222	Cubic
	79.78	1.2	1.2	400	Cubic
CaO-700	32.26	2.77	2.78	111	Cubic
	37.41	2.4	2.41	200	Cubic
	53.86	1.7	1.7	220	Cubic
	64.11	1.45	1.45	311	Cubic
	67.39	1.39	1.39	222	Cubic
	79.71	1.2	1.2	400	Cubic

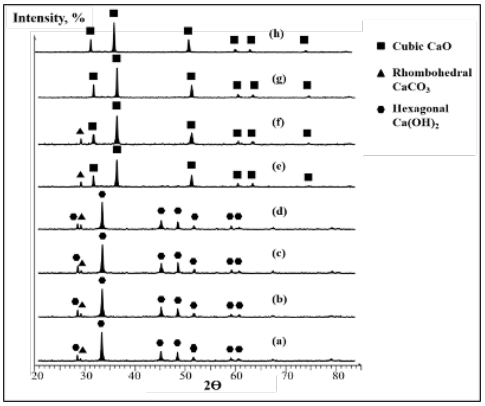

Figure 3. XRD diffractograms of prepared CaO samples at various calcination temperatures of (a) CaO-100 at 100 °C, b) CaO-200 at 200 °C, (c) CaO-300 at 300 °C, (d) CaO-400 at 400 °C, (e) CaO-500 at 500 °C, (f) CaO-600 at 600 °C, (g) CaO-700 at 700 °C, and (h) CaO-800 at 800 °C

explained by the decomposition of $CaCO_3$ to CaO and CO_2 at higher calcination temperature. This treatment subsequently created defect sites as a cavity of prepared CaO to give the increment of its catalyst surface area. As the temperature reached at 800 °C, the SBET slightly decreased due to the sintering effect and particle agglomeration at high temperature. Similar finding was reported previously (Hipólito and Martínez, 2020).

3.1.5 Field Emission Scanning Electron Microscopy- Energy Dispersive X-ray (FESEM-EDX)

The structural changes in CM-$CaCO_3$ during modification was studied by using FESEM micrographs as illustrated in Figure 4 (a). The results demonstrated that CM-$CaCO_3$ was a mixture of bulky particles which had oval shape agglomerates with each other. The morphology of CaO-700 is illustrated in Figure 4(b). The

Table 2. The specific BET surface area, *SBET* of the prepared CaO calcined at various temperatures

Sample	Specific BET Surface Area, *SBET* (m^2g^{-1})
CaO-100	7.9
CaO-200	9
CaO-300	10.4
CaO-400	10.6
CaO-500	10.7
CaO-600	11
CaO-700	11.5
CaO-800	10.6

properties of the resulting modified CaO samples were affected by the calcination temperature of $CaCO_3$. It was found that the large pores were present between CaO particles that bond with each other. A FESEM image for CaO-700 showed the spherical particles coagulated to form agglomerates. Besides, Figure 5 (a) and (b) show the elemental composition by EDX analysis in CM-$CaCO_3$ and CaO-700, respectively. It was found that CM-$CaCO_3$ contained 19.88% weight percentage of carbon, 46.29% of oxygen and 33.83% of calcium, while CaO-700 contained 53.56% of oxygen and 46.44% of calcium.

3.1.6 Basicity of Calcium Oxide Nanoparticles

The basicity of the catalyst is most significant because this site would affect the chemical reactions. Thus, back titration method was performed to determine the basicity of the CaO nanoparticles. The basicity of the prepared CaO was correlated with temperature for decomposition of CM-$CaCO_3$. In the back-titration method, distilled water was added to CaO and left for 24 hours

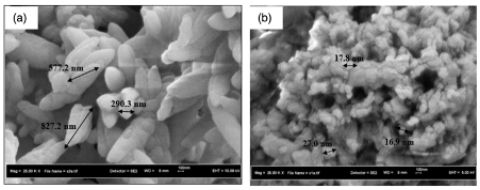

Figure 4. FESEM images of (a) CM-$CaCO_3$ (25kX); (b) CaO-700 (25kX)

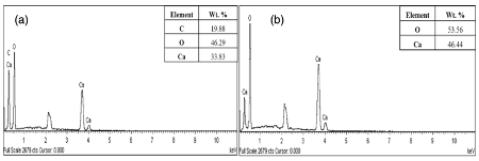

Figure 5. EDX elemental analysis for (a) CM-$CaCO_3$; (b) CaO-700

to make the reaction to occur. Then, the H^+ from water was adsorbed by lone pair of oxygen from CaO surface which corresponds to the amount of basic site (Eq. 1). The desired species, OH^- was obtained by filtering the slurry of extracted proton in CaO. Next, in the neutralization step, the OH^- in clear solution reacted with the HCl to produce water and chloride ion, Cl^- (Eq. 2). While in back titration step, the chloride ion, Cl^- was further reacted with sodium hydroxide, NaOH and phenolphthalein indicator was used to detect the presence of OH^- at the end of the reaction by giving pink color solution (Eq. 3). Figure 6 shows the basicity of the prepared CaO samples at different calcination temperatures.

$$Ca\text{-}O + H^+ \cdots\cdots OH^- \longrightarrow Ca\text{-}O \cdots\cdots H^+ + OH^- \quad (1)$$

$$OH^- + HCl \longrightarrow H_2O + Cl^- \quad (2)$$

$$Cl^- + NaOH \longrightarrow NaCl + OH^- \quad (3)$$

Figure 6 shows that higher calcinations temperature gave the higher basicity which achieved maximum value at 700 °C. At lower temperature, the CaO nanoparticles surface was mostly covered with the OH centres, thus decreased the basicity. By increasing the temperature, more O^{2-} centres started to develop, hence gave a higher basicity. This data is in good agreement with FTIR study that indicated the O-H bonds started to diminish at higher temperature of activation. In a previous study by Yacob et al. (2010), this finding was also in accordance to that used MgO catalyst. It was proven that the basic sites of MgO was detected if the calcinations temperature was above 600 °C which was no free OH^- groups detected by FTIR. Furthermore, basicity of CaO slightly decreased as the temperature reached 800 °C. The fracture of CaO molecular framework and the breaking of crystal structure can describe these results. Moreover, this graph proved that the highest basicity was obtained by CaO-700 sample which about 1.959 mmol/g. Based on the higher amount of basicity, the prepared CaO-700 was selected as heterogeneous base catalyst for the transesterification of rice bran oil to biodiesel.

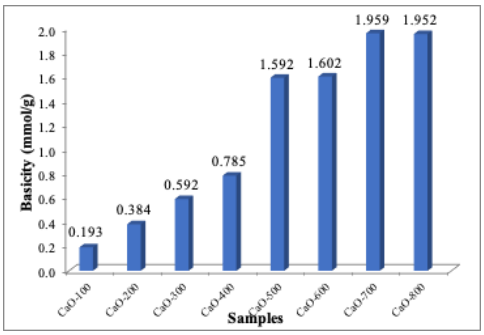

Figure 6. Basicity of the prepared CaO samples at different calcination temperatures

3.2 Biodiesel Analysis

3.2.1 Nuclear Magnetic Resonance (NMR)

NMR is an important analytical technique that is used to determine the quantitative production of biodiesel and the fatty acids mainly the common unsaturated fatty acids such as oleic and linoleic acids (Mantovani et al., 2020). From the previous studies, ^{1}H NMR spectra had been interpreted for soybean oil which were 0.8 ppm related to terminal methyl hydrogen, a strong signal at 1.3 ppm indicates the methylenes of carbon chain, a multiplet signal at 1.6 ppm indicates the β-carbonyl methylenes, a triplet signal at 2.3 ppm related to α-carbonyl methylenes, 3.6 ppm from methoxy group and signal associated to unsaturation at 2.0 ppm, 2.8 ppm and 5.3 ppm indicates to allylic, bis-allylic and olefinic hydrogen respectively (Atabani et al., 2019). The higher conversion of biodiesel was identified if no signal appeared between 4.0 ppm to 5.2 ppm because H-1 and H-3 peaks (refer Figure 7) were corresponded to proton attached at glycerol carbons. Figure 7 shows the transesterification process for biodiesel.

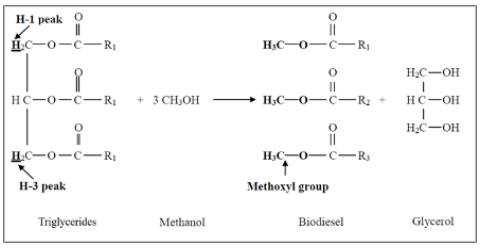

Figure 7. Transesterification process for biodiesel

Figure 8 illustrates ^{1}H NMR spectra of rice bran oil sample, while Figure 9 and Table 3 demonstrate the ^{1}H NMR spectra and peaks assignment for the prepared biodiesel with different times of reaction, respectively. As shown in Figure 8, there was no peak observed at 3.6 ppm that is an important indicator for presence of biodiesel samples. After the transesterification reaction occurred, the peak at 3.6 ppm was determined due to the methoxyl group. The H-1 peak was observed at 4.096 ppm to 4.141 ppm and the H-3 peak was determined at 4.262 ppm to 4.302 ppm from the spectrum shown in Figure 9. In addition, Figure 9 illustrates that peak at 3.6 ppm appeared in all samples of biodiesel due to the

methoxyl group (-O-CH_3) present in the samples. The small H-1 and H-3 peaks at 4.0 ppm to 5.2 ppm which corresponded to protons attached at glycerol carbons can be seen at the reaction of 30 minutes until 150 minutes. Then, when the times of reaction increased, this peak was slightly disappeared due to the higher conversion for biodiesel production.

As explained by Yoo et al. (2010), as transesterification reaction proceeded, H-1, H-2 and H-3 would shift toward higher field as a result of the loss of high electron density of the acyl group, while the proton of acyl group could not shift when one or two of acyl groups migrated from triglycerides (TGs), yielding sn-diglycerides (*sn*-DGs) or sn-monoglycerides (*sn*-MGs). The proton of acyl groups resonates at 0.8-2.9 ppm in TGs (Yoo et al., 2010). Besides, the ratio between the peak of 3.6 ppm from methoxyl groups of methyl esters and 2.3 ppm from α-carbon CH_2 groups of all fatty acid derivatives was calculated for the percentage yield of methyl ester (Shirley and Alesandro, 2008). From the calculation, CaO-700 produced 89.0% methyl esters or biodiesel from rice bran oil. Thus, NMR analysis proved that biodiesel was successfully prepared from single step transesterification of rice bran oil using the prepared CaO-700 catalyst.

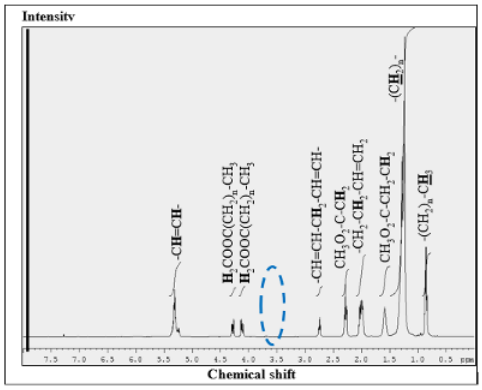

Figure 8. ^{1}H NMR spectrum of rice bran oil sample

Table 3. ^{1}H NMR peaks assignment for biodiesel at different reaction times

Sample	^{1}H NMR regions (ppm)	Peaks assignment
Biodiesel	0.850 – 0.900	-$(CH_2)_n$-CH_3
	1.230 – 1.290	-$(CH_2)_n$-
	1.580 – 1.630	CH_3O_2-C-CH_2-CH_2-
	1.960 – 2.060	-CH_2-CH_2-CH=CH_2
	2.270 – 2.300	CH_3O_2-C-CH_2-
	2.740 – 2.790	-CH=CH-CH_2-CH=CH-
	3.658	-O-CH_3
	4.100 – 4.160	-H_2COOC$(CH_2)_n$-CH_3
	4.250 – 4.320	-H_2COOC$(CH_2)_n$-CH_3
	5.240 – 5.380	-CH=CH-

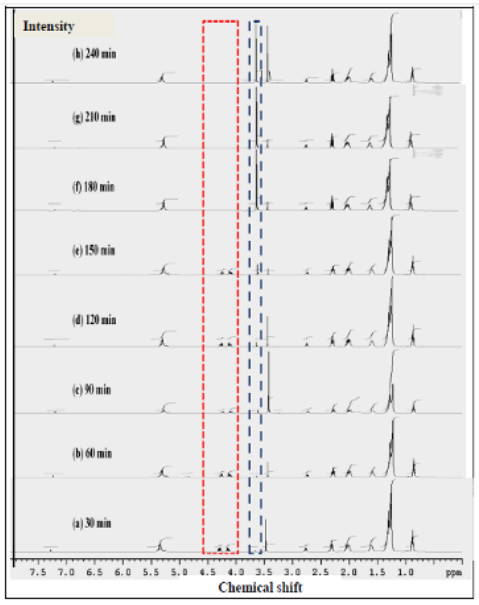

Figure 9. ^{1}H NMR spectra of the prepared biodiesel at different reaction times

3.2.2 Gas Chromatography – Flame Ionization Detector (GC-FID)

Figure 10 illustrates the GC-FID chromatogram of the prepared biodiesel at 60 minutes, while Table 4 shows peaks assignment for retention times from GC-FID chromatogram for the prepared biodiesel. It was found that there were peaks due to the appearances of methyl laurate, methyl tetradecanoate, methyl palmitate, methyl palmitoleate, methyl stearate, methyl oleate, methyl linoleate and methyl tetracosanoate. Based on Table 4, it was found that the most methyl esters that present in the produced biodiesel were methyl tetradecanoate, methyl palmitate and methyl oleate. Thus, GC-FID analysis proved that the biodiesel was successfully prepared by single step transesterification of rice bran oil with methanol and the prepared CaO-700 catalyst.

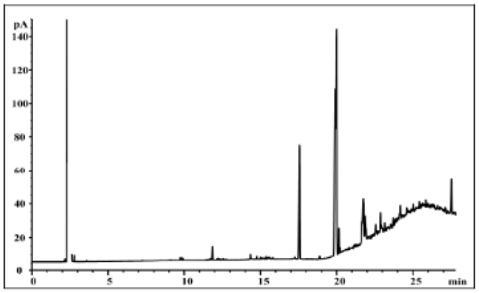

Figure 10. GC-FID chromatogram of prepared biodiesel at 60 minutes

Table 4. Peak assignment for type of fatty acid methyl ester towards retention times from GC-FID chromatogram

Type of fatty acid methyl ester	Retention Times, min
Methyl laurate	14.9
Methyl tetradecanoate	17.5
Methyl palmitate	19.8
Methyl palmitoleate	19.9
Methyl stearate	21.7
Methyl oleate	22
Methyl linoleate	23.4
Methyl tetracosanoate	27.5

3.3 Catalytic Activity

3.3.1 Effect of Catalyst Loading

The effect of catalyst loading towards production of biodiesel using different loadings of catalyst which were 0.5% to 2.5% with 60 minutes reaction times as illustrated in Figure 11. From Figure 11, it shows that 1.0% catalyst loading gave the highest percentage of conversion for biodiesel yield with 89.0%. For 0.5% catalyst loading, the percentage biodiesel production only gave 60.3%, indicating small surface area of the sample. Moreover, incomplete production of FAME was due to an insufficient amount of catalyst as reported by (Olutoye et al., 2016). As increasing the catalyst loading to 1.5% in the reaction, the percentage of biodiesel yield decreased due to its deactivation. The resistance produced by mixing reactant, product and solid catalyst could be the main reason of these results. Such finding was in good agreement with Sulaiman et al. (2020) where it can inhibit the production of biodiesel.

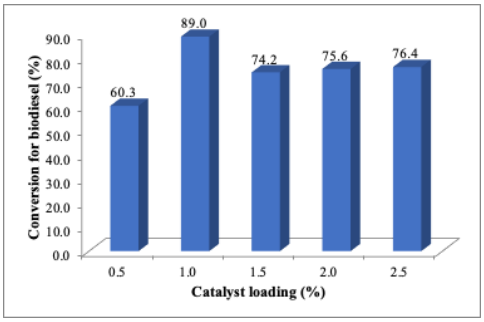

Figure 11. The percentage conversion for biodiesel with different percentage catalyst loadings over CaO-700

3.3.2 Effect of Reaction Times

Figure 12 shows the effect of reaction times towards the production of biodiesel. Interestingly, it was found that the conversion for biodiesel was increased with increasing the reaction times from 30 to 210 minutes and gave 100% conversion of rice bran oil at 210 minutes. This result showed that the low production of biodiesel was found in 30 minutes. Sulaiman et al. (2020) have reported that it is due to the presence of the heterogeneous catalytic mass transfer system. When the reaction time increased to 60 minutes, it can provide more contact times between reactants and catalysts to give high frequent collision. Therefore, high FAME content in the transesterification process can be achieved using an appropriate reaction time while forming adequate quantities of these triglyceride derivatives.

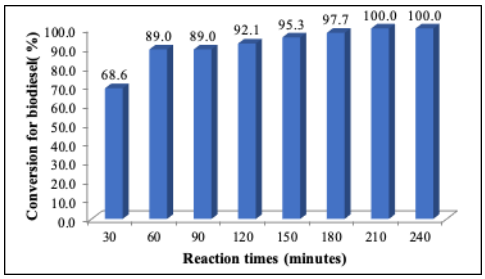

Figure 12. The percentage conversion for biodiesel with different reaction times over CaO-700

4. CONCLUSIONS

The CaO nanoparticles was successfully prepared from commercial calcium carbonate, CM-$CaCO_3$ by thermal decomposition method. The TGA-DTA data showed that there was no more weight loss occurs after 700°C and it verified that $CaCO_3$ was completely decomposed into CaO. The FTIR results supported the TGA-DTA data which indicated the formation of CaO from the decomposition of $CaCO_3$ occurred at 500 to 600°C and completely become CaO at 700°C. Besides, the XRD results confirmed that all the rhombohedral $CaCO_3$ and hexagonal $Ca(OH)_2$ were totally disappeared and only cubic CaO existed at 700°C. The crystallite size of prepared CaO-700 nanoparticles was 38 nm that calculated from Sherrer's equation. It verified that CaO-700 was completely in cubic nanocrystal structure. For nitrogen adsorption analysis, CaO-700 gave the highest BET surface area (11.5 m^2g^{-1}), where catalytic reactions could effectively work at the surface-active sites. In addition, CaO-700 gave the highest basicity with 1.959 mmol/g in order to achieve maximum biodiesel production. In the biodiesel analysis, NMR data confirmed the presence of methoxyl group (-O-CH_3). The percentage biodiesel production that calculated from the ratio between the peak of 3.6 ppm from methoxyl groups of methyl esters and 2.3 ppm from α-carbon CH_2 groups of all fatty acid derivatives found that CaO-700 produced 89.0% of biodiesel at 60 minutes. GC-FID analysis verified that the biodiesel was successfully prepared by single step transesterification of rice bran oil with methanol and prepared CaO-700 as a catalyst with the presence of methyl laurate, methyl tetradecanoate, methyl palmitate, methyl palmitoleate, methyl stearate, methyl oleate, methyl linoleate and methyl tetracosanoate.

5. ACKNOWLEDGEMENT

The authors would like to thank the Ministry of Higher Education (MOHE), Malaysia and Universiti Teknologi Malaysia (UTM) for their financial funding through UTM Transdisciplinary Research Grant (Cost Center No. (Q.J130000.3554.07G57). N.F. Sulaiman thanks UTM for the PDRU Grant Vote No 04E70.

REFERENCES

Atabani, A. E., S. Shobana, M. N. Mohammed, G. Uğuz, G. Kumar, S. Arvindnarayan, M. Aslam, and A. H. Al-Muhtaseb (2019). Integrated valorization of waste cooking oil and spent coffee grounds for biodiesel production: Blending with higher alcohols, FT-IR, TGA, DSC and NMR characterizations. *Fuel*, **244**; 419–430

Aziz, H. M., N. I. Masrom, N. F. Sulaiman, M. K. A. A. Mustajab, and A. R. Yacob (2012). Effect of Hydration-Dehydration Activation on the Basic Strength of Nano Structured Alkaline Earth Metal Calcium Oxide. In *Advanced Materials Research*, volume 383. Trans Tech Publ, pages 3835–3839

Boro, J., D. Deka, and A. J. Thakur (2012). A review on solid oxide derived from waste shells as catalyst for biodiesel production. *Renewable and Sustainable Energy Reviews*, **16**(1); 904–910

Corrêa, R. A. B. L., C. S. Castro, A. S. Damasceno, and J. M. Assaf (2020). The enhanced activity of base metal modified MgAl mixed oxides from sol-gel hydrotalcite for ethylic transesterification. *Renewable Energy*, **146**; 1984–1990

Dawood, S., M. Ahmad, K. Ullah, M. Zafar, and K. Khan (2018). Synthesis and characterization of methyl esters from non-edible plant species yellow oleander oil, using magnesium oxide (MgO) nano-catalyst. *Materials Research Bulletin*, **101**; 371–379

Duan, G., X. Yang, J. Chen, G. Huang, L. Lu, and X. Wang (2007). The catalytic effect of nanosized MgO on the decomposition of ammonium perchlorate. *Powder technology*, **172**(1); 27–29

Hakim, A. L., M. Aznury, and J. M. Amin (2019). Production of Biodiesel from Waste Cooking Oil with Ultrasonic Irradiation Method as Renewable Energy Source. In *Journal of Physics: Conference Series*, volume 1198. IOP Publishing, page 062001

Hattori, H. (2001). Solid base catalysts: generation of basic sites and application to organic synthesis. *Applied Catalysis A: General*, **222**(1-2); 247–259

Hipólito, E. L. and L. M. T. Martínez (2020). Dolomite-supported Cu2O as heterogeneous photocatalysts for solar fuels production. *Materials Science in Semiconductor Processing*, **116**; 105119

Knözinger, E., O. Diwald, and M. Sterrer (2000). Chemical vapour deposition—a new approach to reactive surface defects of uniform geometry on high surface area magnesium oxide. *Journal of Molecular Catalysis A: Chemical*, **162**(1-2); 83–95

Kristl, M., S. Jurak, M. Brus, V. Sem, and J. Kristl (2019). Evaluation of calcium carbonate in eggshells using thermal analysis. *Journal of Thermal Analysis and Calorimetry*, **138**(4); 2751–2758

Li, B., Y. Wei, N. Li, T. Zhang, and J. Wang (2020). Effect of Al (OH) 3 and La 2 O 3 on the Sintering Behavior of CaO Granules via CaCO3 Decomposition. *Science of Sintering*, **52**(2); 1–12

Mantovani, A. C. G., L. T. Chendynski, D. Galvan, F. C. M. Júnior, D. Borsato, and E. D. Mauro (2020). Thermal-oxidation study of biodiesel by proton nuclear magnetic Resonance (1H NMR). *Fuel*, **274**; 117833

Mazaheri, H., H. C. Ong, H. H. Masjuki, Z. Amini, M. D. Harrison, C.-T. Wang, F. Kusumo, and A. Alwi (2018). Rice bran oil based biodiesel production using calcium oxide catalyst derived from Chicoreus brunneus shell. *Energy*, **144**; 10–19

Olutoye, M., S. Wong, L. Chin, H. Amani, M. Asif, and B. Hameed (2016). Synthesis of fatty acid methyl esters via the transesterification of waste cooking oil by methanol with a barium-modified montmorillonite K10 catalyst. *Renewable Energy*, **86**; 392–398

Rathnam, V. M., J. M. Modak, and G. Madras (2020). Non-catalytic transesterification of dry microalgae to fatty acid ethyl esters using supercritical ethanol and ethyl acetate. *Fuel*, **275**; 117998

Shan, R., C. Zhao, P. Lv, H. Yuan, and J. Yao (2016). Catalytic applications of calcium rich waste materials for biodiesel: Current state and perspectives. *Energy Conversion and Management*, **127**; 273–283

Sharma, A., P. Kodgire, and S. S. Kachhwaha (2019). Biodiesel production from waste cotton-seed cooking oil using microwave-assisted transesterification: Optimization and kinetic modeling. *Renewable and Sustainable Energy Reviews*, **116**; 109394

Shirley, N. and B. Alesandro (2008). Use of anhydrous sodium molybdate as an efficient heterogeneous catalyst for soybean oil methanolysis. *Applied Catalysis A: General*, **351**(2); 267–274

Sulaiman, N. F., A. N. N. Hashim, S. Toemen, S. J. M. Rosid, W. N. A. W. Mokhtar, R. Nadarajan, and W. A. W. A. Bakar (2020). Biodiesel production from refined used cooking oil using co-metal oxide catalyzed transesterification. *Renewable Energy*, **153**; 1–11

Yacob, A. R., M. K. A. A. Mustajab, and N. S. Samadi (2010). Physical and basic strength of prepared nano structured MgO. In *2010 International Conference on Mechanical and Electrical Technology*. IEEE, pages 20–23

Yacob, A. R. and N. F. Sulaiman (2012). Hydration dehydration effect on morphology and basic strength of nano-calcium oxide. In *Advanced Materials Research*, volume 488. Trans Tech Publ, pages 967–971

Yoo, S. J., H.-s. Lee, B. Veriansyah, J. Kim, J.-D. Kim, and Y.-W. Lee (2010). Synthesis of biodiesel from rapeseed oil using supercritical methanol with metal oxide catalysts. *Bioresource technology*, **101**(22); 8686–8689

